Optics Communications 285 (2012) 4779–4784

Contents lists available at SciVerse ScienceDirect

Optics Communications

journal homepage: www.elsevier.com/locate/optcom

Effects of 160 keV electron irradiation on the optical properties and microstructure of "Panda" type Polarization-Maintaining optical fibers

Zhang Hong-Chen [a], Liu Hai [a,*], Xue Hui-Jie [b], Qiao Wen-Qiang [a], He Shi-Yu [a]

[a] Space Materials and Environment Engineering Laboratory, Harbin Institute of Technology, Harbin 150001, China
[b] Heilongjiang Key Laboratory for Low Dimensional and Mesoscopic Physics, School of Physics and Electronic Engineering, Harbin Normal University, Harbin 150025, China

ARTICLE INFO

Article history:
Received 14 October 2011
Received in revised form
25 June 2012
Accepted 13 July 2012
Available online 23 August 2012

Keywords:
"Panda" type Polarization-Maintaining optical fiber
Electron irradiation
Si-OH
Irradiation damage

ABSTRACT

In this paper, effects of 160 keV electron irradiated "Panda" type Polarization-Maintaining optical fiber at 1310 nm are investigated by us. Attenuation coefficient induced in optical fiber by electron beams at 1310 nm increases with increase in electron fluence. Electron irradiation-induced damage mechanism are studied by means of CASINO simulation program, the X-ray photoelectron spectroscopy (XPS), electron spin resonance spectrometer (EPR) and Fourier transform infrared spectroscopy (FTIR). The results show that Si-OH impurity defect concentration is the main reason of increasing attenuation coefficient at 1310 nm.

1. Introduction

Polarization-Maintaining optical fiber offer interesting possibility in the field of fiber optic gyroscope (FOG) because of their good Polarization-Maintaining properties and their capability for increment of coherent signal to noise ratio and achieving high precision measurements of physical quantities [1]. Based on Sagnac effect, FOG is solid-state angular velocity measurement equipment [2], which provides accurate information to control the attitude and trajectory of spacecraft, FOG has been widely used in space environment. As for the high precision FOG applied in the field of aerospace, the Polarization-Maintaining optical fiber is a key component of FOG, which increases the precision of FOG compared with the normal optical fiber [3].

The spacecrafts running in orbit are irradiated by broad energy of electron, and long-time irradiation will lead to degradation of the material performance in this environment [4,5]. Electrons with energy less than 200 keV in the material have small range, short term effects of the electron irradiation are unobvious, while the long term effects are more serious [6]. The results show that the Polarization-Maintaining optical fiber of the FOG is most affected in the irradiation environment [7].

"Panda" type Polarization-Maintaining optical fiber is a commonly used silica optical fiber [8,9]. In recent years, the effects of electron irradiation on silica optical fiber are a hot topic and have aroused some attentions due to its application in the field of aerospace [4,5,10–12]. Klose et al. have studied evolution of the 16 MeV energy of electron irradiation-induced optical fiber loss with the fluence, and found the linear behavior within the range of 0–25 Mrad and logarithmic relationship within the range of 25–191 Mrad [12]. Cruz et al. have investigated the Ce- and Nb-doped optical fiber loss induced by 10 MeV electron irradiation. They have found that at 500 Gy dose, the two optical fibers attenuation coefficient at 1550 nm wavelength were 0.070 dB/Gy and 0.045 dB/Gy, respectively, and the irradiation-induced loss changed with the irradiation dose linearly [4]. Yaakob et al. showed that the effects of 2 MeV energy electron irradiation on Ge-doped optical fiber were obvious than that of the Al-doped optical fiber. For the energy 6, 9 and 12 MeV, within 4 Gy dose, Al-doped and Ge-doped optical fiber, the irradiation response were linear relationships with dose, and irradiation response sensitivity of the Ge-doped optical fiber is 2–3% times higher than that of the Al-doped optical fiber [5].

Previous work showed that irradiation-induced degradation of optical fiber is mainly correlated with the structure, composition and production process of the optical fiber [13,14]. Little work about the effects of electron irradiation on the "Panda" type Polarization-Maintaining optical fiber has been reported, especially in the electron energy less than 200 KeV. In this paper, the effects of the 160 KeV electron irradiate on the "Panda" type Polarization-Maintaining optical fiber in FOG are investigated. The evolution of the irradiation-induced loss with electron

* Corresponding author.
E-mail address: hitliuhai@yahoo.com.cn (L. Hai).

0030-4018/$ - see front matter © 2012 Elsevier B.V. All rights reserved.
http://dx.doi.org/10.1016/j.optcom.2012.07.108

fluences is discussed, and the electron energy loss distribution in the optical fiber is calculated by using the CASINO simulation software. X-ray photoelectron spectroscopy (XPS), electron spin resonance spectrometer (EPR) and Fourier transform infrared spectroscopy (FTIR) are used to study the microstructure of the optical fiber before and after irradiation. The transmittance of the silica glass with PMMA and PMMA are analyzed by spectrophotometer and the electron irradiation-induced degradation mechanism in optical fiber is discussed. The results would provide the theoretical and experimental reference for application of the optical fiber in spacecraft.

2. Experimental

2.1. Experimental sample

The "Panda" type Polarization-Maintaining optical fiber used in this work was fabricated by Chinese Wuhan Yangtze Optical Fiber Company. It was prepared by plasma-enhanced chemical vapor deposition method, the fiber type: PM1310-80-16/170, fiber Model: PM1016-B. Their structures are as follows: core (Ge-doped SiO_2), stress zone (B-doped and Ge-doped SiO_2), cladding (SiO_2), coat (Poly methyl methacrylate, that PMMA).

2.2. Irradiation and test equipment

The fiber was irradiated with 160 keV electron at Space Materials and Environment Engineering Evaluation Technology National Key laboratory, Harbin Institute of Technology, China. Sample was placed in a vacuum clamber with the pressure of 10^{-4} Pa. Electron beam density of 0.3 μA/cm^2, the transversal dimensions of the electrons beam of 7×7 cm^2 and irradiation cumulative time of 7 h. With and without irradiation, output and input power of the optical fiber at working wavelength of 1310 nm were measured by AV6331 dual-channel optical power meters, the fiber attenuation coefficient was calculated.

2.3. Analysis methods

After irradiation, CASINO program based on Monte Carlo methods was used to simulate the electron irradiation on the optical fiber, and the energy loss distribution of incident electron in optical fiber was studied. The EPR, XPS and FTIR methods were used to analyse the mechanism of irradiation-induced damage.

XPS (PHI5700, American Perkin-Elmer) with an Al K_α source, EPR (X band A200 paramagnetic resonance spectrometer, German) and FTIR (VECTOR22 Infrared Spectrometer, BRUKER) with the resolution of 2 cm^{-1} and in the range of 400–4000 cm^{-1} were used in this work. UV/VIS double beam spectrophotometer (Lambda 950, American Perkin-Elmer) was used to test transmittance. The transmittance spectra were recorded in the wavelength range of 900–3000 nm and resolution of 5 nm.

3. Experimental results and discussion

3.1. Experimental results

The "Panda" type Polarization-Maintaining optical fibers were irradiated with 160 KeV electron beam, Fig. 1 shows the fluence dependence of attenuation coefficient. The result shows that the attenuation coefficient increases rapidly with increasing the fluence, then slowly, and at the higher fluence there is some saturation in the growth of the attenuation coefficient. For the case of 7×10^{15} cm^{-2} fluence, the magnitude attenuation coefficient changes from 0.426 dB/Km to 45.89 dB/km and indicates a very significant impact of electron irradiation on optical fiber properties.

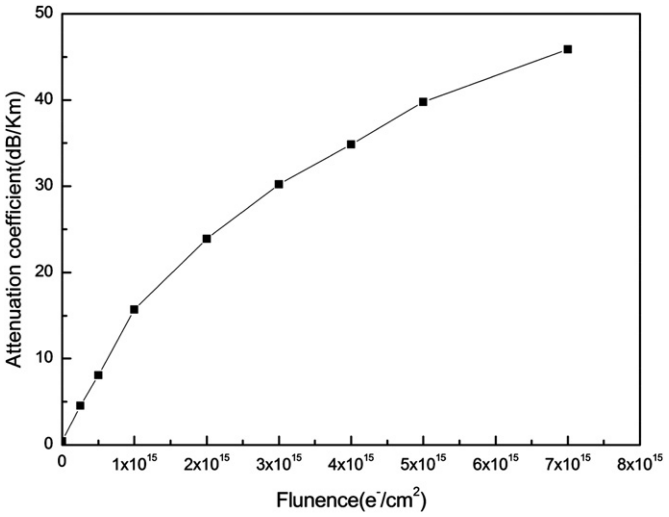

Fig. 1. Extrapolation of "Panda" type Polarization-Maintaining optical fiber attenuation coefficient to fluence.

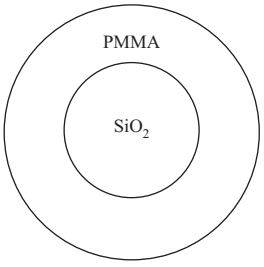

Fig. 2. Schematic of optical fiber structure simplified model.

3.2. Electron energy loss in the fiber

Fiber is a complex system composed of multiple materials. In order to facilitate the use of CASINO program to simulate the process of electron energy loss, the actual structure of the fiber was simplified as shown in Fig. 2. Fiber core, cladding and internal stress zone are made up of silica glass material, and the influence of dope on electron energy loss can be ignored. Hence this part can be regarded as a whole body with thickness of 80 μm in diameter. The average density of SiO_2 layer is selected as 2.32 g/cm^3. Surfacial coat (PMMA) with thickness of 40 μm and density of 1.22 g/cm^3.

Because the radius of single fiber is only 80 μm, it is completely enough to choose a radius of 100 μm electron beam. Following trajectory of 2000 electrons, the energy loss distribution along the radial direction of the "Panda" type Polarization-Maintaining optical fiber irradiated by the 160 keV electron is simulated and calculated by means of CASINO software. Fig. 3 shows distribution of the incident electron energy loss. It is found that electron energy losses mainly lie in a pipeline region of the incident direction, and can completely puncture the coat and fiber core. PMMA absorbs 5–25% of the electron energy. Some part of SiO_2 layer absorbs 50–75% of the electron energy, while 90% can be reached locally in SiO_2.

3.3. Optical fiber irradiation-induced damage studies

3.3.1. FTIR studies on the coat

The FTIR spectra of the PMMA with and without irradiation are shown in Fig. 4. It is found that a new C=C bond absorption peak emerges around 1640 cm^{-1} after irradiation [15].

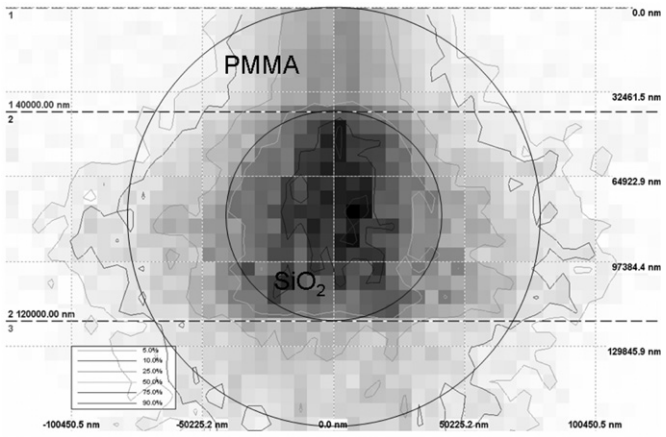

Fig. 3. Distribution of the incident electron energy loss.

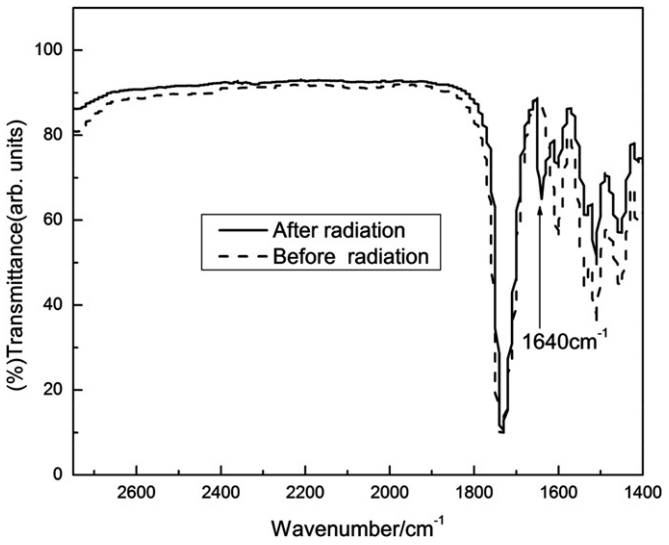

Fig. 4. FTIR spectra before and after electron irradiation.

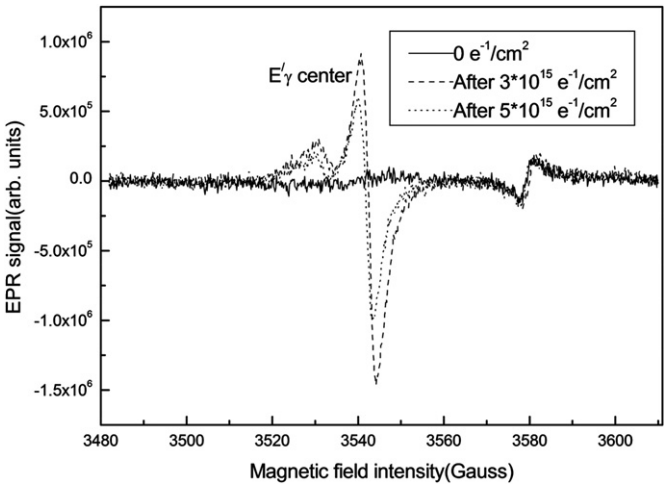

Fig. 5. EPR spectra of unirradiated and electron irradiated cladding and fiber core.

3.3.2. EPR studies

Fig. 5 compares the EPR spectra of unirradiated and electron irradiated cladding and fiber core. As can be seen from Fig. 5, there is an obvious resonance signal that emerges in the electron irradiated sample which is E_{γ}' center in silica glass, the structure is of the form $\equiv Si^{\oplus}$ [16–18]. Moreover, with increasing irradiation fluence, the resonance signal strengthens, which indicates the enhancement of the E_{γ}' center concentration [19].

3.3.3. XPS studies

After stripping the coat, the XPS Si 2p spectra of unirradiated and electron irradiated optical fiber are described in Fig. 6. It is observed that the peak only appears at the binding energy position of 102.2 eV without irradiation, indicates that the silica glass is a complete network structure of the form $\equiv Si–O–Si\equiv$ [20]. In Fig. 6(b), these peaks were divided into two groups, at 99.65 eV and 100.4 eV, corresponding to the Si-H binding energy [21] and the Si-OH binding energy [22], respectively.

Fig. 7 compares the XPS O 1s spectra of the unirradiated and electron irradiated cladding and fiber core. Fig. 7(a) shows a peak at 532 eV, representing bridging oxygen binding energy in SiO_2 network structure [20], and it is agreeing with the Si 2p spectra. After irradiation, new emergence of peaks at 530.35 eV and 533.14 eV binding energies are shown in Fig. 7(b), in which, 530.3 eV is the binding energy of NBO structure in SiO_2 [23], and indicates that the network structure is broken by irradiation and form the structure of $\equiv Si–O^{-}$; 533.14 eV corresponds to the Si-OH binding energy [24]. The origin of hydrogen within silica glass due to the fact that it diffuse from the surface of the coat to inner of the optical fiber in the process of the irradiation.

Stripping the coat of the optical fiber, the main composition of the remaining part is SiO_2. After irradiation, XPS Si 2p spectra and XPS O 1s spectra are shown in Fig. 8. It shows that no new absorption peak appears in XPS Si 2p spectra, while a new absorption peak of 530.4 eV appears in XPS O 1s spectra, represents the binding energy of NBO in SiO_2. However, the absorption peak correlated with Si-OH never appears in both these XPS spectra, e.g. there are no Si-OH impurities in the optical fiber without coat after electron irradiation.

3.3.4. Transmittance analysis

When the electron irradiates on the optical fiber, the electron incidents on the coat material firstly, and then into the SiO_2. Fig. 9(a) shows a plot of the transmittance of PMMA with and without irradiation, it indicates that there is no new absorption peaks appear in the band range of 900–3000 nm with and without electron irradiation, which means that there are no new defects affect the transmittance in the regime of these bands.

The silica glass sheet surface is coated with PMMA and irradiated with electron beam, and the PMMA expose to the irradiation source. We simulate the situation of the irradiated Polarization-Maintaining optical fiber. Fig. 9(b) describes the transmittance of the silica glass with PMMA with and without irradiation covering the band range of 900–2800 nm. It is found that with increasing the electron fluence, transmittance at 1390 nm and 2730 nm decrease gradually due to the existence of Si-OH impurity [27]. It indicates that Si-OH impurity concentration increases with increasing of the electron fluence, and the absorption is more serious at these two wavelengths. Only the Polarization-Maintaining optical fiber at 1310 nm with optical absorption induced by the Si-OH impurity, e.g. the attenuation coefficient increases, and it proves that the attenuation coefficient at 1310 nm increase with increasing the electron fluence.

3.4. Electron irradiation-induced damage mechanism of "Panda" type Polarization-Maintaining fiber

Irradiation-induced defects in material leads to optical fiber power loss after electron irradiation, and the process of the formation and evolution of defects is complex. Studies on the

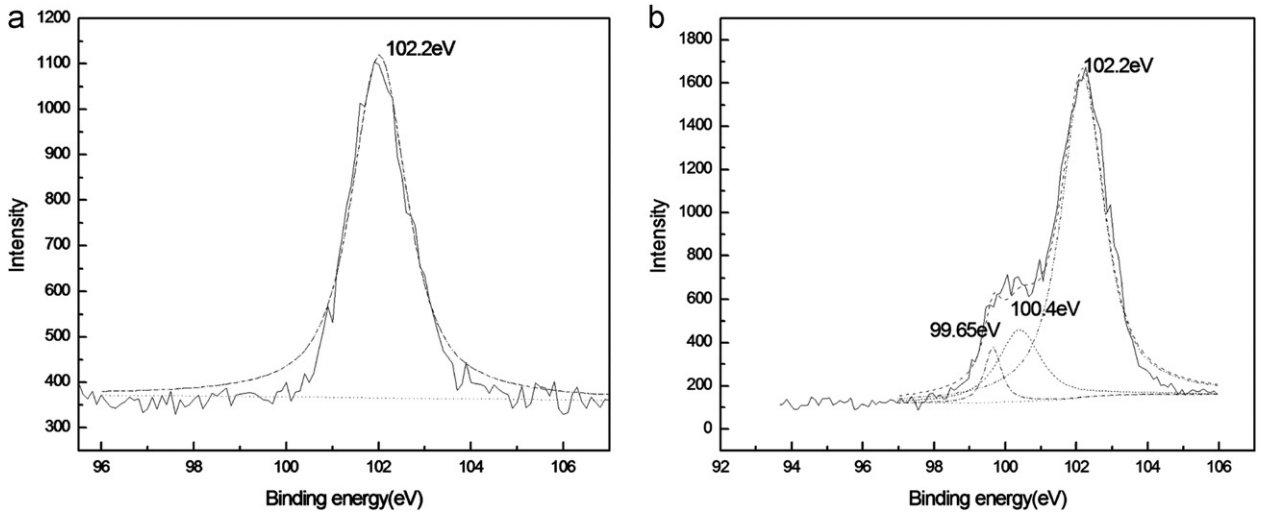

Fig. 6. XPS Si 2p spectra of cladding and fiber core: (a) unirradiated and (b) electron irradiation.

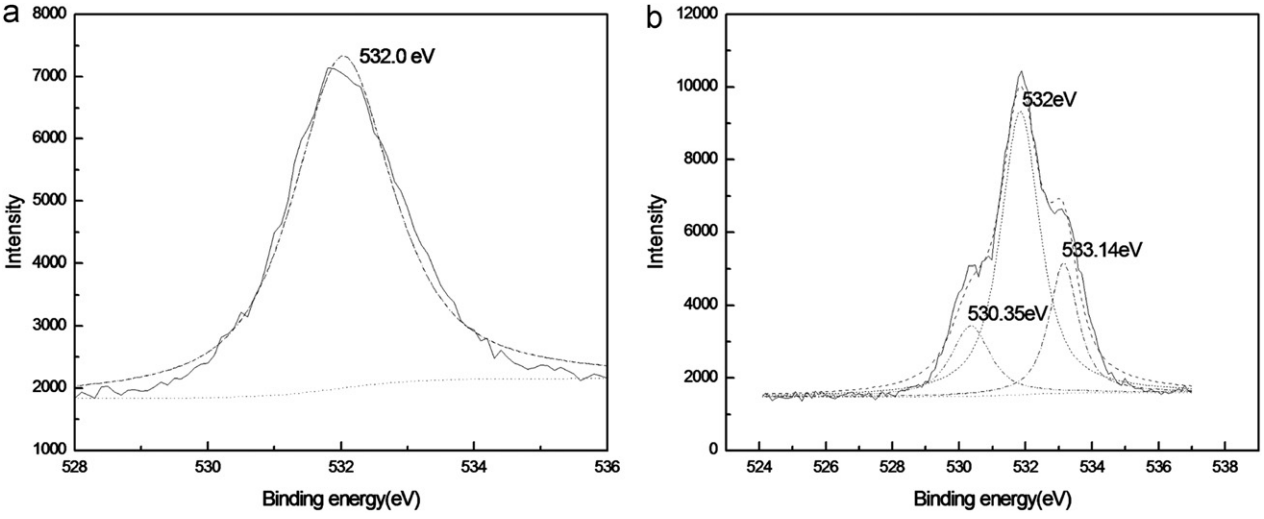

Fig. 7. XPS O 1s spectra for cladding and fiber core: (a) unirradiated and (b) electron irradiation.

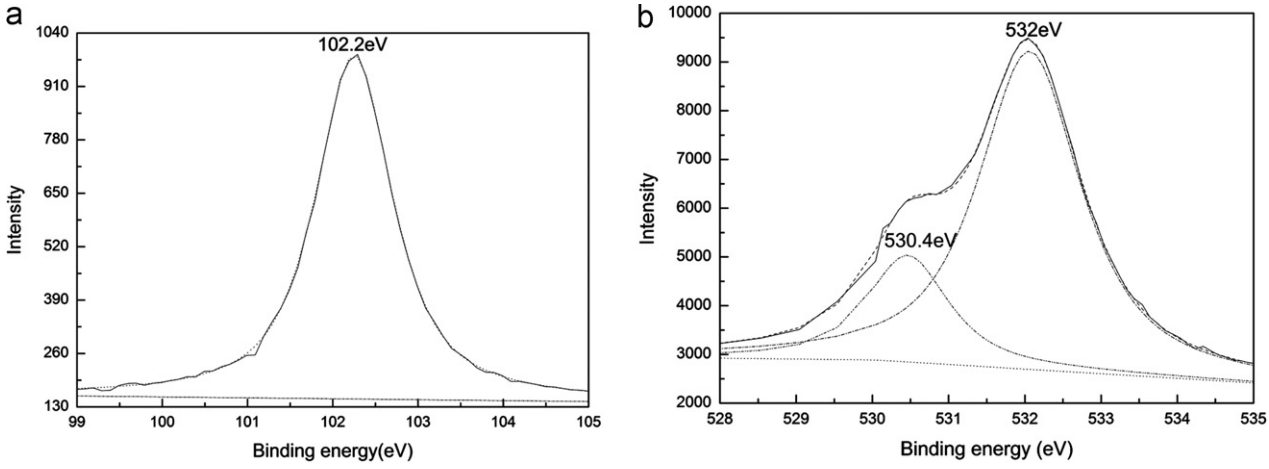

Fig. 8. XPS analytical spectra for cladding and fiber core after electron irradiation: (a) Si 2p and (b) O 1s.

basic law of the process and the internal mechanism not only can help understand adaptability of the optical fiber in the space environment, but also can provide useful guidance for the protection technology in orbit of optical fiber. Adequate results show that irradiation effects on the silica fiber induce Si-OH impurity defects, resulting in the light absorption of optical fiber at 1390 nm, so that the attenuation coefficient increases at 1310 nm [25]. The irradiation effects of the 160 keV electron

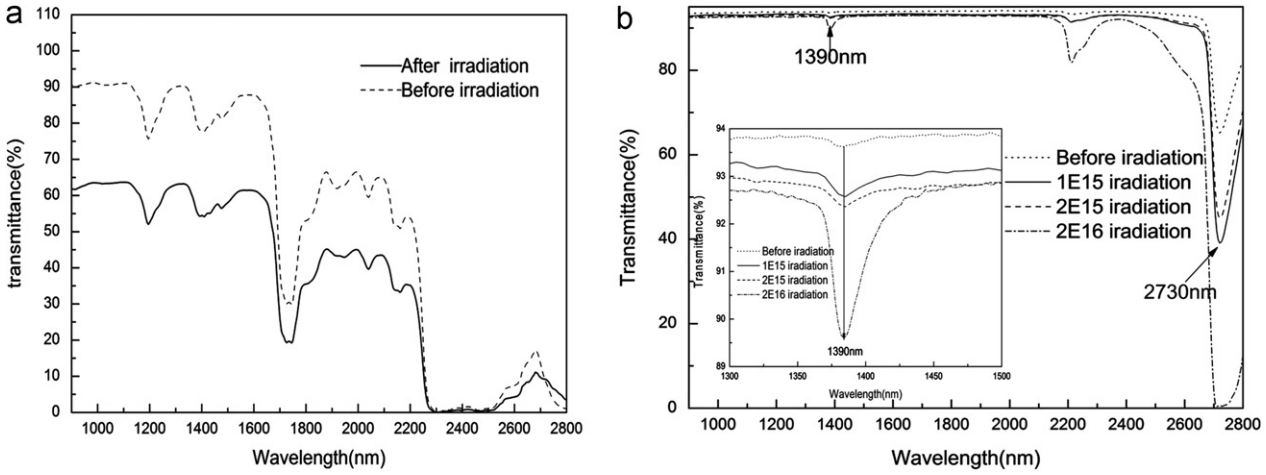

Fig. 9. Transmittance with and without electron irradiation: (a) PMMA and (b) silica glass with PMMA.

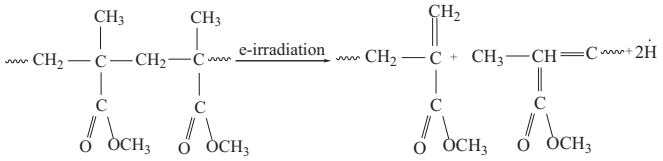

Fig. 10. Schematic representation of the mechanism of electron irradiation-induced structural changes in PMMA.

irradiated "Panda" type Polarization-Maintaining optical fiber have been studied in our experiment, the formation mechanism of the defects within the optical fiber would be explained as follows.

3.4.1. Irradiation effects in coat

Fig. 10 describes the degradation reaction of electron irradiated PMMA [15]. A cleavage of C=H bond in main chain takes place, and reacts with methyl, resulting in the formation of C=C bond, which has been proved by FTIR studies; on the other hand, the methyl involved in reaction release particles $\dot{H}$. CASINO simulation analysis indicates a larger of 160 keV electron irradiation-induced absorption in the coat, leading to the evolution of a large number of particles $\dot{H}$. Because particles $\dot{H}$ are very active, some particles $\dot{H}$ diffuse into the inner of the fiber in the process of irradiation.

3.4.2. Formation of irradiation-induced defects in cladding and fiber core

The CASINO program simulation results show that the incident electrons can pass through the coat and reach the fiber core. As a consequence, larger absorption doses are obtained in the fiber core and cladding. With electron irradiation, strong ionization effect occurs in this region, results in cleavage of the network structure of silica glass, the resulting reaction is as follows [25]:

$$\equiv Si-O-Si \equiv \xrightarrow{Electron} \equiv Si-O^- + \equiv Si^{\oplus} + e \quad (1)$$

The $\equiv$Si–O bond breaks, resulting in the generation of $\equiv Si-O^-$ and $\equiv Si^{\oplus}$ defects. As can be seen from this reaction, electron irradiated optical fiber induce the formation of NBO and E'_γ center defects [17], which has been verified by the XPS and EPR studies.

3.4.3. Formation reaction process of Si-OH defects

XPS studies show a formation of Si-OH structure in electron irradiated silica optical fiber. As there is no hydrogen in silica glass, the only possible origin of hydrogen is coat. Electron irradiation-induced particle $\dot{H}$ in the coat is relatively small, active and easy to diffuse into the fiber by diffusion. The irradiation-induced NBO and E'_γ center defects are unstable, thus, when the particles $\dot{H}$ spread to its vicinity, the following reactions occur [26]:

$$\equiv Si-O^- + \equiv Si^{\oplus} + 2H\cdot \rightarrow \equiv Si-H + \equiv Si-OH \quad (2)$$

In summary, there is Si-OH impurity defects generated in fiber core and cladding due to this reaction. In fact, irradiation-induced loss in material is a very complicate process. Magnitudes of final defects are determined by the two competitive reactions of generation and annihilation process [27]. Under the irradiation process, the Si-OH defects may include decomposition process as follows [28]:

$$\equiv SiOH \rightarrow \equiv SiO^- + H^+ + e^- \quad (3)$$

Therefore, Si-OH impurity defects concentration in the silica optical fiber are closely related to the evolution of the defects.

3.5. Radiation enhanced diffusion (RED)

RED is a very important physical phenomena in irradiation [29]. In materials, the generation of the defect is due to the irradiation-induced damage in material. The diffusion of the impurity in material enhance greatly in this procedure. The irradiation-induced defects generate over saturated concentration on the surface of the material, form big concentration gradient, leading to the accelerating of the diffusion. According to Trap theory, considering the temperature and irradiation, the diffusion coefficient is [30]:

$$D(x,t) = \frac{\lambda^2}{6}\left[\upsilon_0 \exp(-E_T/kT) + \frac{JC(x,t)}{N}\right]\exp(-E_m/kT) \quad (4)$$

where λ is the average jump distance, υ_0 is the jump attempt frequency, J is the particle flux (cm^2/s), C is detrapped gap atomic concentration, N is the number density, E_T and E_m are the trapping and diffusion activation energies, respectively. The first term is heat diffusion; the second term is the irradiation-induced diffusion. The experimental results show that the irradiation can enhance the diffusion, in the case of high particle fluence and large impurity concentration for the same depth of material [30]. In the process of the particle irradiation, diffusion of H in SiO_2 enhances which is bigger than in pure hydrogen gas environment [31]. As shown in Fig. 3, the "Panda" type Polarization-Maintaining optical fiber had a breakdown by 160 kev energy

electron, resulting in the formation of the defects in optical fiber core. Although the optical fiber was only irradiated for 7 h, the defects concentration increases with increasing of the electron irradiation fluence due to the RED effect. In Si-OH of the silica optical fiber, the loss is 54 dB/km at 1390 nm [32]. Thereby, the active particle $\dot{H}$ diffuses into fiber core and form Si-OH, irradiation-induced loss generates in optical fiber.

3.6. Optical fiber attenuation mechanism

In the silica fiber, the basic resonant wavelength of Si-OH bond is 2730 nm which interacts with the resonant wave of Si–O bond. A series of peaks produced in transmission band of the optical fiber, and a greater effective absorption peak is at 1390 nm wavelength [27]. After electron irradiation, Si-OH concentration in optical fiber increases, resulting in 1390 nm absorption peak enhanced and broadened, and 1390 nm absorption peak effect resulting in the increasing of attenuation coefficient at 1310 nm. Therefore, in the "Panda" type Polarization-Maintaining optical fiber at 1310 nm wavelength with electron irradiation, formation and accumulation of Si-OH impurity defect are the natural reasons of the increased attenuation coefficient. Since the formation of the Si-OH defect depends on the NBO and E_γ' center defects, and these irradiation-induced defects are saturated defects, thus the Si-OH defects in the "Panda" type Polarization-Maintaining optical fiber also increase with fluence and tend to saturation gradually, then the values for the attenuation coefficient at 1310 nm wavelength tend to saturation at higher fluence.

4. Conclusions

"Panda" type Polarization-Maintaining optical fiber were irradiated with 160 KeV electron beam and the attenuation coefficient at 1310 nm wavelengths were investigated, the results show that the attenuation coefficient increases with irradiation fluence increasing, and it tends to saturation later. CASINO simulation result indicates that energy loss are observed in both of the PMMA and SiO_2. FTIR studies indicates that electron beam irradiation on the PMMA generate C=C. EPR and XPS studies shows that E_γ' center generated in SiO_2 with electron irradiation. Spectrophotometer studies show that the varies of the Si-OH impurities defects concentration are the main reason of attenuation coefficient change for the electron irradiated "Panda" type Polarization-Maintaining fiber operating at 1310 nm wavelength.

References

[1] X.Q. Wang, C.X. Zhang, J. Jin, N.F. Song, Chinese Optics Letters 9 (2011) 060601.
[2] J. Kang, X. Dong, C. Zhao, W. Qian, M. Li, Optics Communications 284 (2011) 2145.
[3] X. Xu, C. Zhang, J. Song, Optik 120 (2009) 726.
[4] J.L. Cruz, F.L. Valverde, M.V. Andres, J.P. Calatayud, Optics Communications 252 (2005) 286.
[5] N.H. Yaakob, H. Wagiran, I. Hossain, A.T. Ramli, D. ABradley, S. Hashim, H. Ali, Nuclear Instruments and Methods in Physics Research A 637 (2011) 185.
[6] H. Long, H. Fang, S.L. Qi, L.W. Sang, W.Y. Cao, J. Yan, J.J. Deng, Z.J. Yang, G.Y. Zhang, Chinese Physics B 19 (2010) 107307.
[7] B. Tortech, IEEE Transactions on Nuclear Science 55 (2008) 2223.
[8] H.C. Zhang, H. Liu, W.Q. Qiao, H.J. Xue, S.Y. He, Nuclear Instruments and Methods in Physics Research B 274 (2012) 115.
[9] A.N. Trufanov, O.Y. Smetannikov, N.A. Trufanov, Optical Fiber Technology 16 (2010) 156.
[10] A.S. Jacqueline, S.G. Blanco, B. Poumellec, Journal of Non-Crystaline Solids 322 (2003) 284.
[11] S. Hashim, A.S. Ahbabi, D.A. Bradley, M.J. Webb, C. Jeynes, A.T. Ramli, H. Wagiran, Applied Radiation and Isotopes 67 (2009) 423.
[12] H.A. Klose, M. Krause, W. Pfeiffer, J. Rauchfub, G. Sinn, D. Fink, M. Wilhelm, Nuclear Instruments and Methods in Physics Research B 116 (1996) 235.
[13] N.H. Yaakob, H. Wagiran, M.I. Hossain, A.T. Ramli, D.A. Bradley, H. Ali, Applied Radiation and Isotopes 69 (2011) 1189.
[14] S. Hashim, D.A. Bradley, M.I. Saripan, A.T. Ramli, H. Wagiran, Applied Radiation and Isotopes 68 (2010) 700.
[15] Ismayil, V. Ravindrachary, R.F. Bhajantri, S.D. Praveena, B. Poojary, D. Dutta, P.K. Pujari, Polymer Degradation and Stability 95 (2010) 1083.
[16] S. Agnello, G. Buscarino, F.M. Gelardi, Journal of Non-Crystaline Solids 351 (2005) 1787.
[17] G. Buscarino, S. Agnello, Journal of Non-Crystalline Solids 353 (2007) 577.
[18] A. Alessi, S. Agnello, D.G. Sporea, C. Oproiu, B. Brichard, F.M. Gelardi, Journal of Non-Crystalline Solids 356 (2010) 275.
[19] G. Buscarino, G. Vaccaro, S. Agnello, F.M. Gelardi, Journal of Non-Crystalline Solids 355 (2009) 1092.
[20] S.H. Lee, S. Jeong, J. Moon, Organic Electronics 10 (2009) 982.
[21] I.H. Tan, M.L.P.D Silva, N.R. Demarquette, Journal of Materials Chemistry 11 (2001) 1019.
[22] W.H Koo, S.H Choi, H.K Baik, S.M. Lee, S.J. Lee, Electronic Materials Letters 1 (2005) 107.
[23] Q.Y. Wang, H.B. Geng, S.Y. He, D.Z. Yang, Z.H. Zhang, X.W. Qin, Z. Li, Nuclear Instruments and Methods in Physics Research B 267 (2009) 2489.
[24] M. Feng, Y.G. Li, J.F. li, J. Li, X.G. Zhang, K.C. Lu, H.J. Wang, Chinese Physics Letters 22 (2005) 1137.
[25] K. Kajihara, L. Skuja, M. Hirano, H. Hosono, Physical Review Letters 89 (2002) 135507.
[26] Y. Nagasawa, H. Ishida, F. Soeda, A. Ishitan, I. Yoshii, K. Yamamoto, Mikrochimica Acta I (1998) 431.
[27] Q. Wei, S.Y. He, H. Liu, D.Z. Yang, Acta Optica Sinica 25 (2005) 83.
[28] Y. Morita, W. Kawakami, IEEE Transactions on Nuclear Science 36 (1989) 584.
[29] G.J. Dienes, A.C. Damask, Journal of Applied Physics 29 (1958) 1713.
[30] Y. Yamamura, Nuclear Instruments and Methods in Physics Research B 153 (1999) 410.
[31] F. Corni, A. Monelli, G. Ottaviani, R. Tonini, G. Queirolo, L. Zanotti, Journal of Non-Crystalline Solids 216 (1997) 71.
[32] T. Ning, K.S. Hu, H.J. Fu, Acta Physica Sinica 39 (1990) 82.